

CFD-Validierung einer Statorschaufel mittels MRV zur Ermittlung des optimalen Turbulenzmodells

CFD validation of a stator vane using MRV to find the optimal turbulence model

C. Wüstenhagen¹, C. Domnick², M. Bruschewski¹, S. Grundmann¹

¹Universität Rostock, Lehrstuhl Strömungsmechanik, Albert-Einstein-Str. 2, 18059 Rostock

²MAN Energy Solutions SE, Steinbrinkstrasse 1, 46145 Oberhausen

Magnet Resonanz Velocimetrie, Turbinenschaufelkühlung, Turbulenz, Data Matching
magnetic resonance velocimetry, turbine blade cooling, turbulence, data matching

Zusammenfassung

Computational Fluid Dynamics (CFD) ist das gängige Werkzeug in der Turbomaschinenindustrie, um interne Kühlsysteme von Turbinenkomponenten zu analysieren und zu optimieren. Um das geeignete Turbulenzmodell für eine bestimmte Anwendung zu wählen, werden experimentelle Validierungsdaten benötigt. In dieser Studie wird ein Statorschaufel-Kühlsystem vorgestellt, das drei Serpentin mit Rippenturbulatoren und Hinterkantenausblausung besitzt. Die Kühlströmung wird mit verschiedenen Ansätzen zur Modellierung der Turbulenz simuliert. Insgesamt wurden 22 CFD-Simulationen für Turbulenzmodelle der Reynolds-Averaged-Navier Stokes (RANS) durchgeführt. Zum Vergleich wurde eine Simulation ohne Verwendung eines Turbulenzmodells und eine Scale Adaptive Simulation (SAS) evaluiert. Diese CFD-Daten wurden mit dreidimensionalen Magnetresonanz-Velocimetrie (MRV) Messungen einer skalierten Nachbildung der Schaufel unter Verwendung einer Data Matching Routine verglichen. Die Abweichungen wurden anhand globaler Fehlermetriken bewertet, was zu einer Rangfolge der Turbulenzmodelle führt. Bei ausgewählten Modellen wurden zusätzlich die lokalen Fehlergrößen bewertet, um die Modellierungsfehler in der Querströmung zu untersuchen. Im Allgemeinen schnitten k - ϵ -basierte Modelle weniger gut ab als k - ω -basierte Modelle. Das Ein-Gleichungs-Modell von Spalart-Allmaras lieferte etwas überraschend das beste Kosten-Nutzen-Verhältnis.

Abstract

Computational Fluid Dynamics (CFD) is the common tool in the turbomachinery industry to analyze and optimize internal cooling systems of turbine components. To choosing the appropriate turbulence model for a particular application experimental reference data are needed. In this study, we present a stator vane cooling system consisting of a three-pass serpentine with rib turbulators and trailing edge ejection. The cooling flow is simulated using different approaches for modelling the turbulence. In total, 22 CFD simulations were carried out using turbulence models from the Reynolds-Averaged-Navier-Stokes (RANS) framework. For comparison, one simulation without using a turbulence model and a Scale-Adaptive-Simulation (SAS) were carried out. These CFD data were compared to three-dimensional Magnetic Resonance Velocimetry (MRV) measurements of a scaled replica of the vane using a data matching routine. The deviations were evaluated using global error metrics leading to a ranking of the turbulence models. On selected models, the local error quantities were additionally evaluated to investigate the modelling error in the secondary flow. In general, k - ϵ -based models performed not as good as k - ω -based ones. The one-equation Spalart-Allmaras model somewhat surprisingly yielded the best cost-benefit ratio.

Introduction

The operating temperatures of modern gas turbines have to be as high as possible to reach high efficiencies. This poses a challenge to the durability and service life of the turbine components. Excessive cooling of the components, e.g. the turbine blades, addresses this challenge. The inner cooling flow of turbine blades has a special significance here. The design of interior cooling passages is often characterized by serpentine equipped with pin fins or ribs in various designs. Most studies, experimental or numerical, examine generic models, but there are studies addressing realistic serpentine recently (Chen et al., 2022; Wang et al., 2021).

Design studies, to achieve optimal internal cooling flows, are almost always performed using computational fluid dynamics (CFD) studies based on low-effort models that yield much faster response times than experimental studies. The selection of the best turbulence model for a given optimization task is often based on experience. Turbulent flows with various deflections, as we find in internal cooling systems of turbine blades, are challenging for most turbulence models used for numerical simulations.

Experimental data are needed to validate the simulations. Magnetic resonance velocimetry (MRV) is a predestined measurement technique for this purpose due to its ability to measure time averaged three-dimensional three-component velocity fields in a relatively short time without optical access. The resolution of MRV is not sufficient to resolve the boundary layer, but yielding millions of data points, MRV can provide extensive experimental validation data for the macroscopic turbulent flow outside the boundary layers. In addition, it is possible with MRV to determine the Reynolds Stress Tensor (RST) and thus the turbulence intensity.

This study presents a real internal cooling geometry from a stator vane currently used in a modern, small industrial gas turbine. The investigated cooling system consists of a three-pass, rib-turbulated serpentine with trailing edge ejection. MRV measurements of the velocity field and the RST of the internal cooling flow are performed using a scaled replica of the original vane which is perfused with water. Using the Reynolds similarity these experimental data can be compared to numerical simulations. All numerical simulations are performed using Ansys CFX. To find the optimal turbulence model for this application, 23 simulations using different turbulence models with different parameters such as the curvature correction are performed.

Materials and Methods

MRV Measurements

The MRV measurement technique places some requirements to the experimental setup. Instead of air flow, the model must be perfused using a fluid, which must contain a measurable magnetic resonance signal. For this application, incompressibility can be assumed, since the Mach number of internal cooling flows usually does not increase above 0.3. Therefore, purified water with copper sulfate is used to perfuse the stator vane model.

The model of the stator vane is scaled 3.9 times the size of the original vane to achieve a relatively high resolution and moderate flow velocities to minimize the misregistration error of the MRV measurement. Misregistration is the flow displacement that occurs at high velocities, because the signal changes position during the measurement process. This leads to distorted data sets if the displacement exceeds the voxel length and is one of the most serious cause of errors of MRV measurements.

The vane model was manufactured using the multi jet fusion process with polyamide powder, because models must not contain metallic components. Polyamide as well as Poly(methyl

methacrylate) (PMMA) yield similar magnetic susceptibilities compared to water and are therefore suitable materials for the manufacturing of MRV models (Wapler et al., 2014).

PMMA was used to install a settling chamber, the in- and outlet as well as a transparent window at the trailing edge for visual inspection.

The flow loop consists of a frequency-controlled 1.5 kW pump, a 300-liter tank and hoses that connected the system with the settling chamber of the stator vane model. The outlet hose is then connected to the inductive flow meter SM7020 (ifm electronic GmbH, Essen, Germany) and a resistance temperature detector (standard PT100 sensor). The tank was heated by a submerged heat exchanger connected to a 2 kW electric heater. The water and copper sulfate solution was set to have a constant temperature of 40°C and the flow rate was adjusted to 54.6 L/min in order to reach the target Reynolds number at the inlet of $Re = 45.000$, calculated using the hydraulic diameter. The bulk inlet velocity resulted in $u_{bulk} = 0.73 \text{ m/s}$.

The MRV and RST measurements were performed using a conventional 3T whole-body MRI scanner (Magnetom Trio, Siemens Healthineers, Erlangen, Germany) with a maximum gradient amplitude of 40 mTm^{-1} and a maximum gradient slew rate of $200 \text{ Tm}^{-1}\text{s}^{-1}$.

First, the three-dimensional velocity field of the inner cooling system of the vane was measured using a velocity-encoded phase-contrast gradient-recalled echo sequence (Nishimura et al., 1991). With a resolution of $(0.75 \text{ mm})^3$, 3.2 million data points were acquired to map the inner cooling system of the vane model. The velocity encoding value (VENC) was set so 3 m/s to yield a good agreement between measurement precision and low turbulence related signal attenuation. A lower VENC yields a lower baseline uncertainty but turbulent dephasing becomes stronger, which can yield high local uncertainties. The time-averaged velocity field results from the average of ten individual measurements. To cancel out velocity errors from secondary velocity sensitivities, scans without flow were performed before and after the velocity measurements. These data sets were fitted on a statistical model representing these velocity errors and then subtracted from the velocity data.

Second, the RST measurement was performed on a two-dimensional slice at the inlet section using the encoding scheme of Schmidt et al. (2021) that uses multiple VENC values to increase the precision of RST data. The resolution was set to $(0.75 \text{ mm})^2$ and 5 mm slice thickness. The number of averages varied using the different VENCs. The parameters for both, MRV and RST measurements are shown in table 1.

Table 1: Parameters of the MRV and RST measurement.

	3D mean velocity (MRV)	2D turbulence (RST)
Voxel size in mm^3	0.75 x 0.75 x 0.75	0.75 x 0.75 x 5
FOV in mm^3	312 x 254 x 108	72 x 72 x 5
VENC in m/s	3	0.23 to 4.7, seven VENC in total
No. of Averages	10 (+2 "Flow Off")	256 to 128
Echo time in ms	2.9	5.5
Repetition time in ms	5.1	8.0
Flip angle in °	20	20
Bandwidth in Hz/px	800	700

The turbulent kinetic energy k is an important boundary condition for numerical simulations of turbulent flows and can be derived from the components of RST as follows

$$k = \frac{1}{2} \cdot (\overline{u'_x u'_x} + \overline{u'_y u'_y} + \overline{u'_z u'_z}). \quad (1)$$

All measurement data were processed with Matlab (The MathWorks, Inc., Natick, MA, USA) and visualized in Paraview (Kitware Inc., Clifton Park, NY, USA).

CFD Simulations

The velocity field inside the three-pass system was calculated with the commercial CFD Solver Ansys CFX 19.2 using 22 turbulence models of the Reynolds-Averaged-Navier-Stokes framework, one laminar calculation and one Scale-Adaptive-Simulation (SAS). The computational domain comprises the 3-pass-system and the outflow bores. It is discretized by an unstructured tetrahedral grid with a prismatic sublayer. The total node count is 34.4 million nodes and the sublayer has a height of 15 elements. The non-dimensional height of the first element (y^+) is less than 3. The grid was taken from a high-quality engine calculation for which grid independence was reached in an internal study. The high-resolution scheme, which has an adaptive order of accuracy, was used to solve the equations. In Wüstenhagen et al., 2022 it is shown that this scheme works, in a very similar case, close to second order. At the inlet of the computational domain a mass flow boundary condition was set. With this mass flow rate, an inlet Reynolds number of 45,000 is reached. At the end of the discharge holes at the trailing edge, a pressure boundary condition was set. For all cases, the boundary conditions are identical.

A rather simple approach to model the effects of turbulence are eddy viscosity models. Here, different models that calculate the eddy viscosity based on one or two differential equations are applied. Two rather simple models that are used here are the Model by Spalart and Allmaras (1992) and the eddy viscosity transport equation (evte) by Menter 1997. The more advanced two equation turbulence models are widely used in the turbomachinery industry as they offer a good tradeoff between accuracy and computational effort. Here the $k-\epsilon$ model (Launder and Spalding 1974) the $k-\omega$ (Wilcox 1988) and the Shear-Stress-Transport model (Menter 1994) are applied.

To capture special effects of turbulent flow the Shear-Stress-Transport model (SST) can be extended by the curvature correction and a transition model that predicts laminar turbulent transition in the boundary layer. The curvature correction which is described in Spalart and Shur (1997) shall predict the increase of turbulence generation occurring in highly curved flows. It can be tuned by a limiter function which was varied in this study. A widely used model to capture laminar-turbulent transition is the $\gamma-\theta$ -transition model by Langtry and Menter (2005), which was also applied in this study.

More sophisticated than the previous eddy-viscosity models are Reynolds-stress models (RSM) which predict the 6 individual components of the Reynolds-stress tensor. Both algebraic and differential RSM were applied. The algebraic models are based on the EARSM model by Wallin and Johansson (2000) that obtains the Reynold-stress tensor from a two equation model. The EARSM can be either used to extend the baseline model (BSL) by Menter (1994) or the $k-\epsilon$ -model. In the used code Ansys-CFX, the tensor basis for the model was slightly changed to the formulation of Apsley and Leschziner (1998). As the BSL-model is based on the $k-\omega$ -model, curvature correction and the $\gamma-\theta$ - transition model can be applied on this model and are evaluated in this study.

The SSG Reynolds-stress model (Speziale, Sarkar and Gatski, 1991) is the Reynolds-stress model that is applied in this study. As differential equations for the six components of the Reynolds-stress tensor are solved, this model is more complex and hence more computational intense.

Finally, the SAS was performed. In this simulation, the large-scale turbulence is solved and small-scale turbulence is modeled. The implementation is described in detail in Egorov and Menter (2008). As turbulence is resolved, this approach is inherently time resolving and hence very computational intense. For the investigations presented here, the computed transient values are time-averaged for comparison with the other CFD approaches and the experimental data.

Data Matching Routine

To quantitatively compare the MRV measurement to the various CFD simulations, a data matching routine is used, which is presented in Wüstenhagen et al. (2021). After applying an alignment algorithm, the data sets are on the same coordinate system and can therefore be directly compared point by point. In a first step, global error metrics are evaluated to get an overview of the general performance of the used turbulence model in this particular problem. The mean absolute error (MAE) is calculated as follows:

$$\text{MAE} = \left| \frac{1}{N} \sum (u_{CFD}(\mathbf{r}) - u_{MRV}(\mathbf{r})) \right| \times 100\% \quad (2)$$

with u_{CFD} and u_{MRV} being the velocity vectors normalized with the bulk inlet velocity, respectively. Note, that this normalization and comparison is possible due to the Reynolds similarity. The corrected root mean square error is the second global error metric

$$\text{cRMSE} = \sqrt{\frac{1}{N} \sum (u_{CFD}(\mathbf{r}) - u_{MRV}(\mathbf{r}))^2 - \sigma_u^2} \times 100\% \quad (3)$$

with the measurement uncertainty σ_u (Bruschewski et al., 2016).

A high MAE can be interpreted as a higher systematic error whereas a high cRMSE indicates higher local deviations.

Selected simulations are studied in more detail by investigating the local error fields. The local absolute error is calculated component-wise for all three velocity components. Using the norm of the three-component local absolute error, the direction of the velocity vectors is taken into consideration in contrast to using the velocity magnitude only. (Wüstenhagen et al., 2022). The component wise absolute error is

$$\text{AE}_X(\mathbf{r}) = |u_{X,CFD}(\mathbf{r}) - u_{X,MRV}(\mathbf{r})| \times 100\% \quad (4)$$

and the absolute error, calculated from the individual velocity components, is then

$$\text{AE}_C(\mathbf{r}) = \sqrt{\text{AE}_X(\mathbf{r})^2 + \text{AE}_Y(\mathbf{r})^2 + \text{AE}_Z(\mathbf{r})^2}. \quad (5)$$

The percentage error is displayed by the arctangent percentage error

$$\text{AAPE}_X(\mathbf{r}) = \frac{4}{\pi} \arctan \left(\left| \frac{u_{X,CFD}(\mathbf{r}) - |u_{X,MRV}(\mathbf{r})|}{u_{X,MRV}(\mathbf{r})} \right| \right) \times 100\%, \quad (6)$$

which also is calculated using the magnitude of the component wise percentage errors

$$\text{AAPE}_C(\mathbf{r}) = \sqrt{\text{AAPE}_X(\mathbf{r})^2 + \text{AAPE}_Y(\mathbf{r})^2 + \text{AAPE}_Z(\mathbf{r})^2}. \quad (7)$$

Using the arc tangent function causes the error from 0 to infinity to be mapped on a scale from 0 to 200.

Results and Discussion

First, the RST measurement results are examined. The turbulence intensity

$$I = \sqrt{\frac{2}{3}k} / u_{bulk} \quad (8)$$

is calculated from the results of the RST measurement. The mean turbulence intensity at the 2D inlet slice of the vane is 6.7%. This agrees well enough with the 5% turbulence intensity assumed in the CFD simulations.

The velocity field of the vane, measured with MRV, is shown in figure 1 in form of streamlines to get an overview of the flow characteristics in the vane model. It can be seen that the fluid accelerates in the first u-bend due to a slight cross section narrowing. After the first u-bend a large recirculation zone is formed. This effect is reinforced by the connection of the second

and third pass. After the second u-bend another recirculation zone can be seen, that is smaller than after the first u-bend. The flow towards the trailing edge should be viewed with caution, because it is displayed by just a few voxels due to the narrowing cross section.

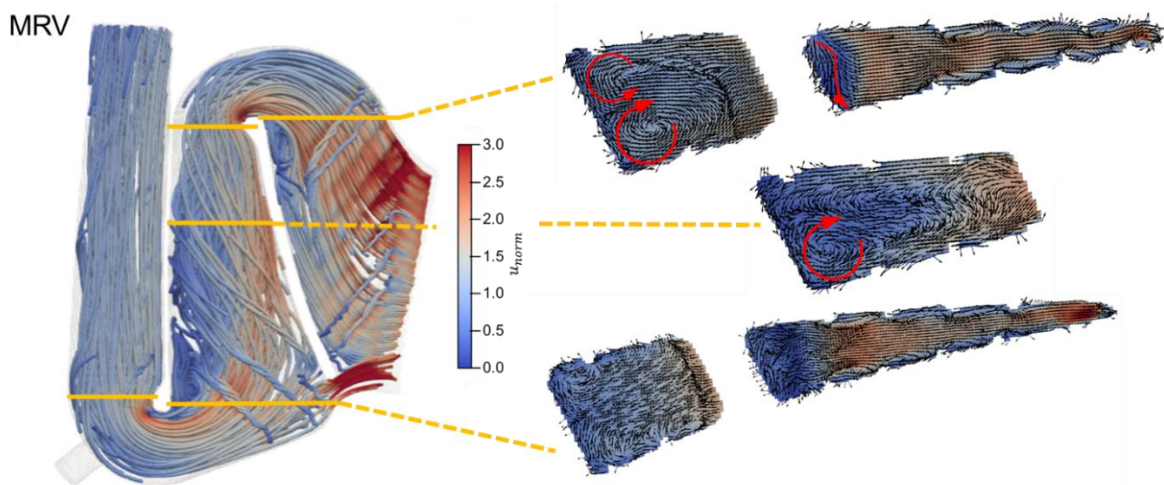


Figure 1: Flow characteristics of the vane model that was measured with MRV, displayed by streamlines on the left. Secondary flow at three slices on the right with vortexes displayed by red arrows.

The results of the evaluation of the global errors can be seen in table 2. The turbulence models are grouped in one equation, two equations, algebraic Reynolds stress, differential Reynolds stress, and other models. The group of 'other models' consists of the SAS and the laminar calculation (termed None).

Table 2: Global error metrics MAE and cRMSE of the 24 numerical simulations. Left: sorted by MAE, right: sorted by cRMSE.

	turbulence model	MAE [%] ↓	cRMSE [%]	turbulence model	MAE [%]	cRMSE [%] ↓
	SAS-ZFLES	0,93659	13,4032	SA	1,0041	12,1892
	SA	1,0041	12,1892	SST	1,0343	12,2529
	SST	1,0343	12,2529	kepsEARSM_gt	1,1901	12,3866
	EARSM_gt_cc80.00	1,0453	13,6981	EARSM_gt	1,1903	12,3909
	evte	1,0588	12,7742	SST_gt	1,1131	12,4692
	SST_gt_cc1.25	1,0723	13,1741	EARSM_ft	1,1393	12,4758
	EARSM_gt_cc20.00	1,0823	13,4918	Kw	1,2229	12,6372
	SST_ft	1,0837	12,9050	SST_gt_cc20.00	1,1979	12,6611
	BSL_ed	1,0957	13,0115	Evte	1,0588	12,7742
1 eq.	SST_gt_cc5.00	1,0981	13,4331	EARSM_gt_cc1.25	1,13	12,8219
2 eq.	SST_gt	1,1131	12,4692	SST_ft	1,0837	12,9050
alg. RST	EARSM_gt_cc5.00	1,1176	13,3209	Keps	1,1591	12,9241
diff. RST	Rngkeps	1,1177	13,4746	BSL_ed	1,0957	13,0115
other	SSG	1,1261	13,8726	SST_gt_cc80.00	1,2978	13,1431
	EARSM_gt_cc1.25	1,13	12,8219	SST_gt_cc1.25	1,0723	13,1741
	EARSM_ft	1,1393	12,4758	SST_ft_cc80.00	1,2759	13,2583
	Keps	1,1591	12,9241	EARSM_gt_cc5.00	1,1176	13,3209
	None	1,1895	15,6566	SAS-ZFLES	0,93659	13,4032
	kepsEARSM_gt	1,1901	12,3866	SST_gt_cc5.00	1,0981	13,4331
	EARSM_gt	1,1903	12,3909	Rngkeps	1,1177	13,4746
	SST_gt_cc20.00	1,1979	12,6611	EARSM_gt_cc20.00	1,0823	13,4918
	kw	1,2229	12,6372	EARSM_gt_cc80.00	1,0453	13,6981
	SST_ft_cc80.00	1,2759	13,2583	SSG	1,1261	13,8726
	SST_gt_cc80.00	1,2978	13,1431	none	1,1895	15,6566

It can be seen that the one equation models somehow show good results in the evaluation of both, the absolute and the percentage, global error. The k-w-SST model without any configurations regarding the transition model or the curvature correction shows good results as well. Nevertheless, the deviations of MAE and cRMSE are small for a majority of the turbulence models. Therefore, the local flow characteristics and error metrics will now be considered. For reasons of clarity, a selection of turbulence models is used to investigate the local errors on two selected slices of the secondary flow. In figure 2 it can be seen that the vortex of the large recirculation zone of the second passage is predicted well by all turbulence models. The simulation without turbulence model fails to predict the flow characteristics as expected. Considering the errors AE_C and $AAPE_C$, it seems like the evte model predicts the flow in this selected slice best. The turbulence models SA, k- ω -SST and k- ϵ also provide a good agreement.

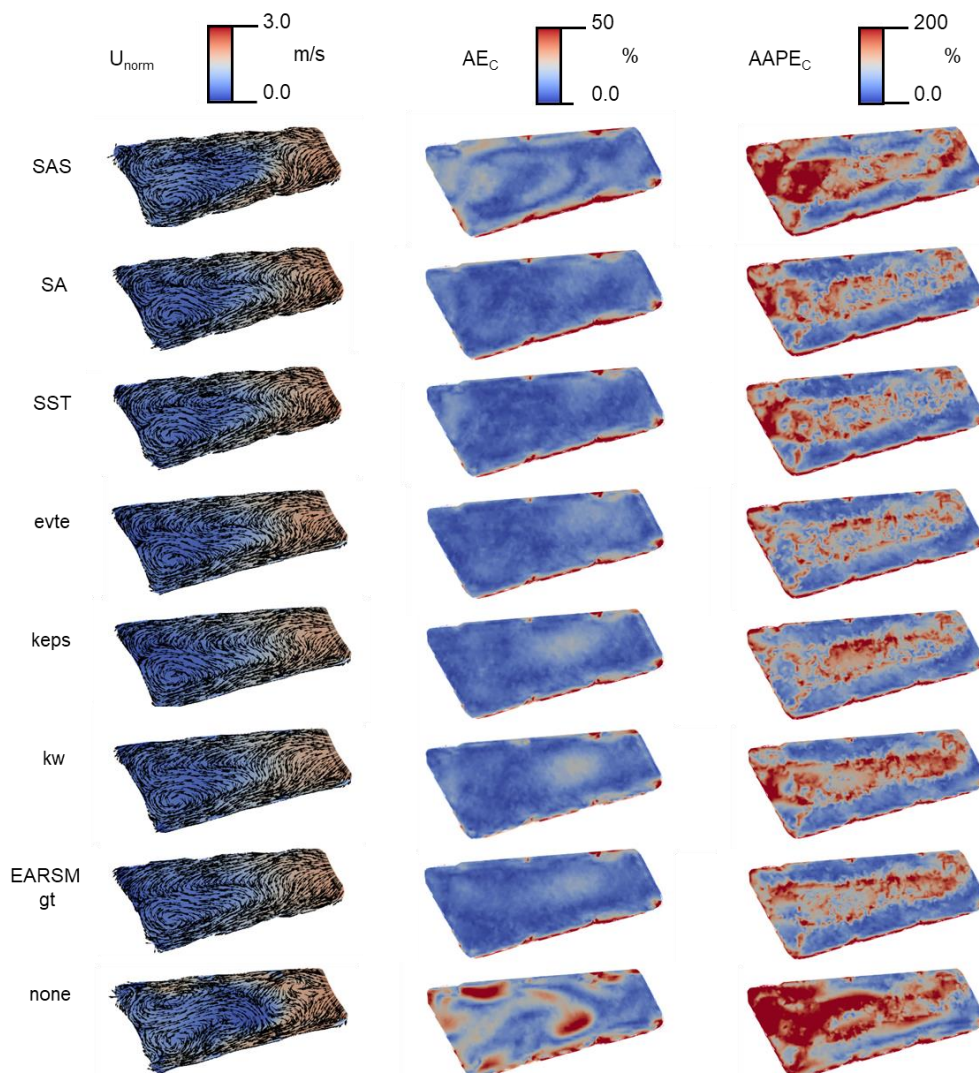


Figure 2: Normalized velocity u_{norm} and errors AE_C and $AAPE_C$ at the middle slice of the middle passage.

Figure 3 shows the secondary flow right before and behind the second u-bend. MRV data shows two equally large vortices before the u-bend, see figure 1. This flow feature can be seen in the CFD data using all turbulence models except the computationally expensive SAS that shows a larger and a smaller vortex. Using no turbulence model, does not predict this feature, as before. All turbulence models over predict the velocities opposite of the vortices.

Looking at the Slice right after the u-bend, it can be seen that the velocity recirculation zones runs in slightly different directions. Some turbulence models predict the flow alongside the wall as *evte* or *k-ε*, and some models, as *SA* or *k-ω-SST*, predict the flow to make a slight turn before reattaching to the wall, as the MRV data shows, see figure 1. This slight difference can be seen in the local error field AE_C . The turbulence models *SAS*, *k-ω* or *EARSM_gt* overestimate the extension of the recirculation zone.

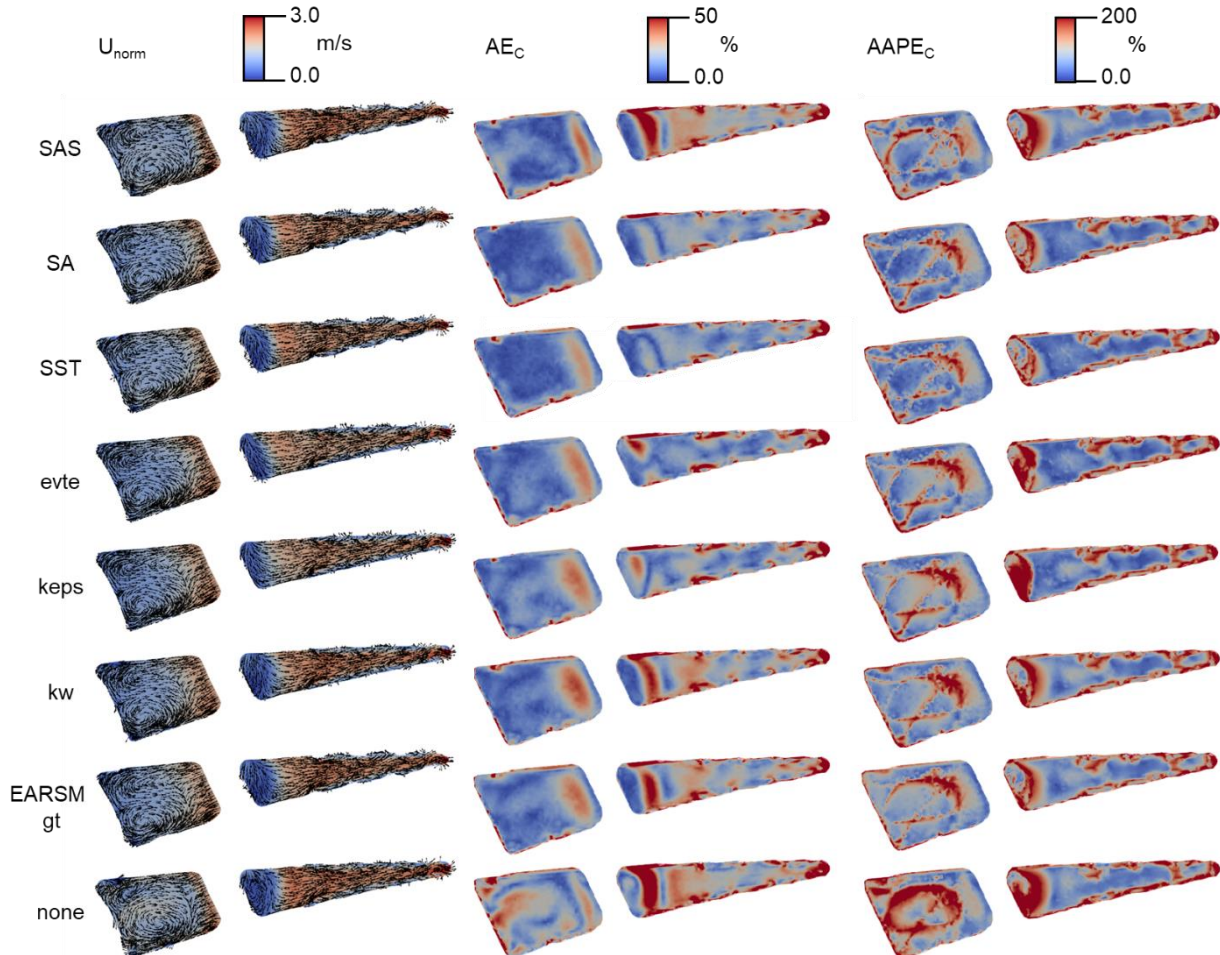


Figure 3: Normalized velocity u_{norm} and errors AE_C and $AAPE_C$ bevor and after the second u-bend.

High errors, that can be seen with AE_C and $AAPE_C$, that occur at all walls in figure 2 and 3 and especially in the last-mentioned towards the trailing edge should be neglected. They most likely occur because MRV cannot dissolve the boundary layer.

On the example of the *k-ω-SST* model, the influence of the transition model and the curvature correction is investigated, see figure 4. Looking at the cross section before the u-bend, it can be seen that the plain *SST* as well as both, $\gamma-\theta$ and fully turbulent transition models, reach a high agreement with the MRV data. Using curvature correction values of 1.25 and 5.0 in combination with the $\gamma-\theta$ transition model lead to a shift of the upper vortex to the right which does not match with the MRV measurement. Therefore, higher AE_C and $AAPE_C$ values can be seen. A curvature correction value of 20.0 somewhat predicts the location of the vortexes right, but overestimates the velocities at the opposite wall. This effect agrees well with the lower *cRMSE* value and higher *MAE* value in comparison to the smaller curvature correction values, see table 2. Curvature correction values of 80.0 lead to a large overestimation of the velocities at the right wall. Even if the vortex orientation is well predicted, the high velocities lead to smaller vortexes, resulting in higher AE_C and $AAPE_C$ errors.

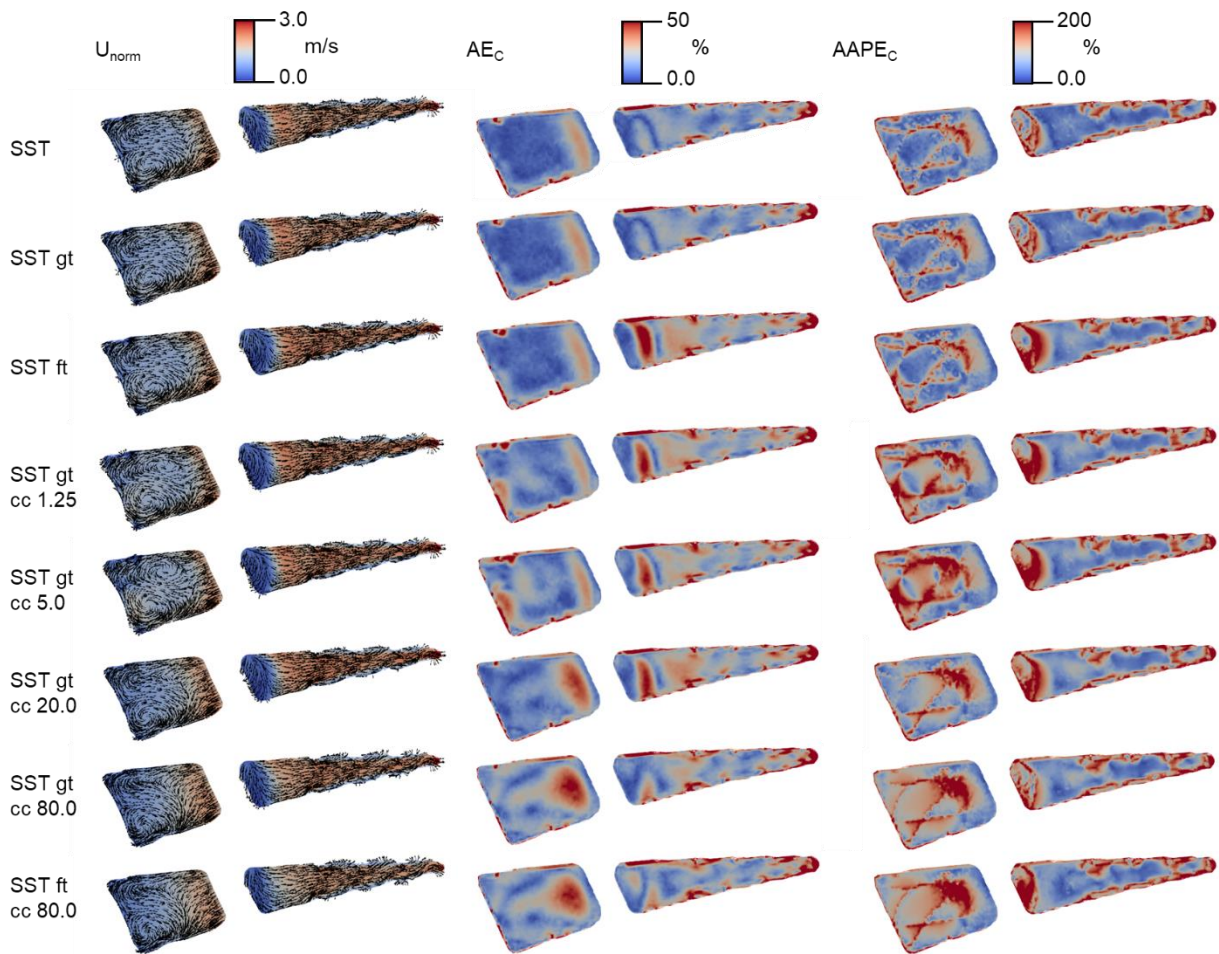


Figure 4: k- ω -SST model with fully turbulent and γ - θ transition models with different curvature correction values.

Looking at the cross section after the u-bend, it can be seen that the fully turbulent transition model without curvature correction and the γ - θ transition model with curvature correction values from 1.25 to 20.0 lead to high absolute and percentage errors in the recirculation zone. A curvature correction of 80.0 with fully turbulent as well as γ - θ transition model lead to higher errors at the ribs and an inferior prediction of the recirculation zone compared to the plain SST and the SST model with as γ - θ transition model. They reach the best agreement. Visually, there is no difference to tell, but the global errors suggest, that the plain SST model performs best in this comparison.

Conclusion

Numerical simulations and experimental MRV measurements of the flow field in a three-pass internal cooling system of a high-pressure turbine vane were presented. The simulations were performed using various RANS turbulence models including the variation of transition models and the curvature correction parameter. Using MRV, the three-dimensional time-averaged velocity field within the vane model was measured with sufficient resolution and accuracy to provide a comprehensive database for CFD validation. Global and local errors in the CFD data were evaluated via a three-dimensional data comparison approach.

A focus was on the secondary flow at important locations of the vane model. Almost all turbulence models showed weaknesses in the flow detachment and reattachment regions. Regarding the curvature correction and the choice between fully turbulent or γ - θ transition model it seems like the SST model predicts the flow in this application best without curvature cor-

rection or transition model. Nevertheless, the variation of these parameters will be investigated in a future study. In conclusion, k - ω -based models seem to better predict the flow field as k - ϵ -based turbulence models in this particular application. The one-equation Spalart-Allmaras model somewhat surprisingly yielded the best cost-benefit ratio.

Acknowledgements

Essential parts of the work presented herein were supported within the framework of RoBoFlex AP3.6 under grant number FKZ 03EE5013J of the German Federal Ministry of Economic Affairs and Climate Action. The authors are grateful for the financial support from MAN Energy Solutions SE and acknowledge MAN for the permission to publish this paper. The responsibility for the content lies solely with the authors.

References

- Wüstenhagen, C., John, K., Langner, S., Brede, M., Grundmann, S., Bruschewski, M. 2021:** „CFD validation using in-vitro MRI velocity data – methods for data matching and CFD error quantification”, *Computers in Biology and Medicine* (131), doi.org/10.1016/j.combiomed.2021.104230
- Bruschewski, M., Wüstenhagen, C., Domnick, C., Krewinkel, R., Shiau, C. C., Grundmann, S., Han, J. C. 2022:** “Assessment of the flow field and heat transfer in a vane using magnetic resonance velocimetry, thermochromic liquid crystals and cfd” *Turbo Expo: Power for Land, Sea, and Air*. American Society of Mechanical Engineers.
- Nishimura, D. G., Jackson, J. I., and Pauly, J. M., 1991:** "On the nature and reduction of the displacement artifact in flow images", *Magnetic resonance in medicine*, 22(2), pp. 481-492.
- Schmidt, S., John, K., Kim, S. J., Flassbeck, S., Schmitter, S., and Bruschewski, M., 2021:** "Reynolds stress tensor measurements using magnetic resonance velocimetry: expansion of the dynamic measurement range and analysis of systematic measurement errors", *Experiments in Fluids*, 62(6), pp. 1-17.
- Wüstenhagen, C., Domnick, C., John, K., Bruschewski, M., and Grundmann, S., 2022:** "MRI investigations of internal blade cooling flow and CFD optimization through data matching", *Proceedings of ASME Turbo Expo 2022 Turbomachinery Technical Conference and Exposition*, Rotterdam, The Netherlands, June 13-17, 2022.
- Bruschewski, M., Freudenhammer, D., Buchenberg, W.B., Schiffer, H.P., and Grundmann, S., 2016:** „Estimation of the measurement uncertainty in magnetic resonance velocimetry based on statistical models“, *Exp Fluids* 57:83. DOI: 10.1007/s00348-016-2163-3
- Wapler, M.C., Leupold, J., Dragonu, I., von Elverfeld, D., Zaitsev, M., and Wallrabe, U., 2014:** „Magnetic properties of materials for MR engineering, micro-MR and beyond“, *Journal of Magnetic Resonance*, 242, 233–242.
- Chen, I. L., Sahin, I., Wright, L. M., Han, J. C., and Krewinkel, R., 2022:** "Heat Transfer in a Rotating, Blade-Shaped, Two-Pass Cooling Channel with Various 45-Deg Rib Orientations" *Journal of Thermal Science and Engineering Applications*, 14(9), 091009.
- Wang, X., Xu, H., Wang, J., Song, W., and Wang, L., 2021:** „High pressure turbine blade internal cooling in a realistic rib roughened two-pass channel“, *International Journal of Heat and Mass Transfer*, 170. 121019.
- Spalart, Philippe, and Steven Allmaras, 1992:** "A one-equation turbulence model for aerodynamic flows." 30th aerospace sciences meeting and exhibit. Reno NV, S. 439.
- Menter, Florian R. 1997:** Eddy viscosity transport equations and their relation to the k - ϵ model." *Journal of Fluids Engineering* 119(4) 876-884.

Launder B. E., Spalding, D. B. 1974: "The numerical computation of turbulent flow." *Computer Methods in Applied Mechanics and Engineering* 3 (1974) pp. 269-289

Wilcox David C., 1988: "Multiscale model for turbulent flows." *AIAA journal* 26(11) pp. 1311-1320.

Menter, Florian R. 1994: "Two-equation eddy-viscosity turbulence models for engineering applications", *AIAA journal*, 32(8) pp. 1598-1605.

Spalart, P.R., and Shur, M.1997: "Curvature correction," On the sensitization of turbulence models to rotation and curvature" *Aerospace Science and Technology*, 1(5), pp. 297-302.

Langtry, R.B., Menter, F.R., 2005: "Transition Modeling for General CFD Applications in Aeronautics", *AIAA paper* 2005-522

Wallin, Stefan, and Arne V. Johansson 2000: "An explicit algebraic Reynolds stress model for incompressible and compressible turbulent flows." *Journal of fluid mechanics* 403 (2000): 89-132.

Apsley, David D., and Leschziner, Michael A., 1998: "A new low-Reynolds-number nonlinear two-equation turbulence model for complex flows." *International Journal of Heat and Fluid Flow* 19.3 (1998): 209-222.

Speziale, Charles G., Sutanu Sarkar, and Thomas B. Gatski., 1991: "Modelling the pressure-strain correlation of turbulence: an invariant dynamical systems approach." *Journal of fluid mechanics* 227 (1991): 245-272.

Egorov, Y., Menter, F. R., 2008: "Development and Application of SST-SAS Turbulence Model in the DESIDER Project," in *Adv. in Hybrid RANS-LES Modeling*. Berlin: Springer Verlag, pp. 261-270